Ceramics International, Volume 45, Issue 9, June 2019, pp. 11375-11381
DOI:10.1016/j.ceramint.2019.03.001

Superior energy-storage properties in (Pb,La)(Zr,Sn,Ti)O_3 antiferroelectric ceramics with appropriate La content

Y Dan, K Zou, G. Chen, Y Yu, Y Zhang, QF Zhang, Y Lu, Q Zhang, Y. He

Abstract

Antiferroelectric (AFE) ceramics based on Pb(Zr,Sn,Ti)O_3 (PZST) have shown great potential for applications in pulsed power capacitors because of their fast charge-discharge rates (on the order of nanoseconds). However, to date, it has been proven very difficult to simultaneously obtain large recoverable energy densities W_{re} and high energy efficiencies η in one type of ceramic, which limits the range of applications of these materials. Addressing this problem requires the development of ceramic materials that simultaneously offer a large ferroelectric-antiferroelectric (FE-AFE) phase-switching electric field E_A, high electric breakdown strength E_b, and narrow polarization-electric field (*P-E*) hysteresis loops. In this work, via doping of La^{3+} into $(Pb_{1-1.5x}La_x)(Zr_{0.5}Sn_{0.43}Ti_{0.07})O_3$ AFE ceramics, large E_A and E_b due to respectively enhanced AFE phase stability and reduced electric conductivity, and slimmer hysteresis loops resulting from the appearance of the relaxor AFE state, are successfully obtained, and thus leading to great improvement of the W_{re} and η. The most superior energy storage properties are obtained in the 3 mol% La^{3+}-doped $(Pb_{1-1.5x}La_x)(Zr_{0.5}Sn_{0.43}Ti_{0.07})O_3$ AFE ceramic, which simultaneously exhibits at room temperature a large W_{re} of 4.2 J/cm^3 and a high η of 78%, being respectively 2.9 and 1.56 times those of $(Pb_{1-1.5x}La_x)(Zr_{0.5}Sn_{0.43}Ti_{0.07})O_3$ AFE ceramics with $x = 0$ (W_{re} = 1.45 J/cm^3, η = 50%) and also being superior to many previously published results. Besides, both W_{re} and η change very little in the temperature range of 25–125 °C. The large W_{re}, high η, and their good temperature stability make the $Pb_{0.955}La_{0.03}(Zr_{0.5}Sn_{0.43}Ti_{0.07})O_3$ AFE ceramic attractive for preparing high pulsed power capacitors useable in various conditions.

Keywords

Relaxor antiferroelectrics, La^{3+} content, Energy-storage density, Energy efficiency,

Temperature stability

1. Introduction

In recently, much attention and research interest has been devoted to energy-storage devices in order to meet the needs of social sustainable development [1,2]. Present energy-storage devices mainly consist of electrochemical capacitors, batteries, dielectric capacitors and fuel cells. In all these energy-storage devices, dielectric capacitors have faster charge-discharge rate (<1 μs), more excellent fatigue endurance, and lower energy loss, and thus are widely used in electromagnetic guns, particle beam accelerators, laser technology, and hybrid electrical vehicles, which require a rapid and gigantic energy release so as to acquire large pulsed power [3,4]. Dielectric materials used in dielectric capacitors are classified into four categories: ferroelectrics (FEs), linear dielectrics (LDs), antiferroelectrics (AFEs), and relaxor ferroelectrics (RFEs). Generally, AFEs can exhibit more superior energy-storage properties than FEs because of their near-zero remnant polarization, and than LDs and RFEs due to their larger saturation polarization [5,6]. Thus, in recent years, energy-storage properties of AFE materials, especially (Pb,La)(Zr,Sn,Ti)O3 AFE systems on account of their wide AFE phase region, have been widely studied and reported [[7], [8], [9], [10], [11]].

For AFE materials, as presented in Fig. 1, the total energy-storage density (W), the recoverable energy-storage density (Wre), and the energy efficiency η can be respectively defined as [12]:(1)W=Wre+Wloss=∫0PmaxEdP(uponcharging),

(2)Wre=−∫PmaxPrEdP(upondischarging), (3)η=WreW×100%, where the Pmax and Pr are respectively the maximum and the remnant polarization, and the E is the applied external electric field. From Fig. 1 and Eqs. (1), (2), it is clear that increasing EA, the electric breakdown strength (Eb), Pmax, and decreasing the electrical hysteresis (ΔE = EF − EA) improve Wre and η, respectively. Thus, AFEs which exhibit high EA, Eb, Pmax and slim double P-E hysteresis loops are best choice for developing and preparing dielectric capacitors possessing superior energy-storage properties.

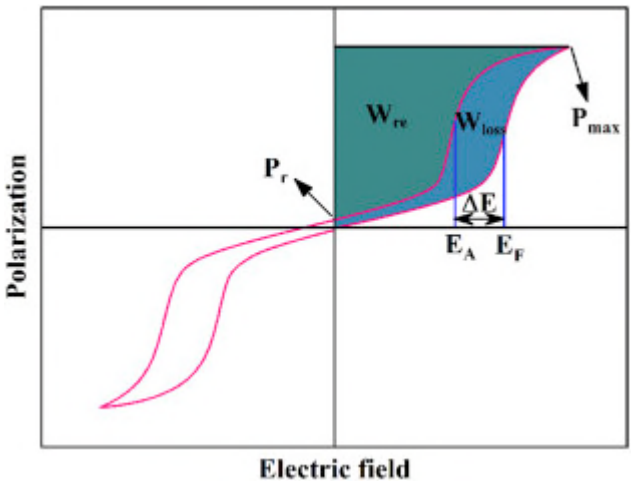

Fig. 1. Schematic diagram showing energy-storage properties of AFE materials.

In (Pb,La)(Zr,Sn,Ti)O3 AFE materials, the contents of Zr, Ti, Sn, and La all have obvious effects on EA, Pmax, Eb, and ΔE [9,11,13,14]. For example, upon continuously increasing the La3+ content, the phase structure of (Pb,La)(Zr,Sn,Ti)O3 ceramics at room temperature transforms from AFE state to relaxor AFE state with slimmer hysteresis loops, larger EA, and higher Eb [15,16]. This is good for improving Wre and η. However, to date, only two research groups have reported how the La3+ content affects energy-storage characteristics of (Pb,La)(Zr,Sn,Ti)O3 AFE ceramics. Because of inappropriate Zr:Sn:Ti ratios, the maximum Wre is only 1.47 J/cm3, which is far less than that required for practical applications of dielectric capacitors [13,17]. Very recently, we found that (Pb,La)(Zr,Sn,Ti)O3 AFE ceramics with high Sn content have a superior energy-storage capacity because the introduction of elemental Sn can make the P-E hysteresis loops slimmer and increase Eb [11]. Thus, adding more La3+ into these AFE ceramics with high Sn content may lead to a larger Wre and a higher η.

Based on above discussion, in this work, we study the influence of the La3+ content on the phase structure, surface morphology, and energy-storage characteristics of (Pb1-1.5xLax)(Zr0.5Sn0.43Ti0.07)O3 AFE ceramics with high Sn content. With the optimum La3+ content, the ceramic exhibits simultaneously a large Wre of 4.2 J/cm3 and a high η of 78%,

which are respectively 2.9 and 1.56 times greater than those of (Pb1-1.5xLax)(Zr0.5Sn0.43Ti0.07)O3 AFE ceramics with $x = 0$ ($W_{re} = 1.45$ J/cm3, $\eta = 50\%$) and are also superior to many previously reported results. Furthermore, we attempted to correlate quantitatively the EF, EA, and ΔE with the temperature variation.

2. Experimental procedures

(Pb1-1.5xLax)(Zr0.5Sn0.43Ti0.07)O3 (PLZST) ($x = 0$, 0.5%, 1%, 1.5%, 2.5%, 3%, 4%, 5%) AFE ceramics were prepared via the conventional ceramic fabrication technique, using PbO (≥99%), La2O3 (≥99.99%), TiO2 (≥98%), SnO2 (≥99.5%) and ZrO2 (≥99%) as raw materials. These powders were weighed on the basis of above chemical formula, ball milled and calcined at 870 °C for 2 h. The powders were ball milled again, pressed into discs of 1.5 mm thickness and 11.5 mm diameter, and sintered at 1230 °C for 2 h. In order to measuring electrical properties, the sintered ceramics were covered with silver electrodes at 550 °C for 10 min.

The apparent density of the sintered sample was measured by the Archimedes method. The phase and crystal structure of the ceramics were examined by the powder x-ray diffraction (XRD; D8 Advance; Bruker, Karlsruhe, Germany). The micrographs of the fresh ceramics were performed by the scanning electron microscopy (SEM; JSM 6510LV; Jeol, Tokyo, Japan). Elemental mappings were done using a SEM (FE-SEM; SIGMA 500; Zeiss, Oberkochen, Germany). The polarization-electric field (P-E) hysteresis loops were characterized at 10 Hz with a precision ferroelectric measurement system (PolyK Technologies, State College, Pennsylvania, USA).

3. Results and discussion

Fig. 2(a) gives XRD patterns of PLZST ceramics with different La^{3+} contents at the room temperature. The results clearly demonstrate that all ceramics have a pure perovskite structure without secondary or impure phase. To characterize more clearly the phase structure of PLZST ceramics, we examine fine scanning XRD patterns in the 2θ range of 43°–45°, as given in Fig.

2(b). Two split peaks of (200) and (002) are apparently shown, indicating a tetragonal phase structure of the ceramics. In addition, upon increasing the La3+ content from x = 0 to x = 5%, both the (200) and (002) peaks shift to higher angles, indicating an decrease in the lattice parameters, as shown in Fig. 3. The decrease of lattice parameters a and c with increasing La3+ content in the PLZST ceramics is attributed to smaller ionic radius of La3+ (1.36 Å) compared with Pb2+ (1.49 Å).

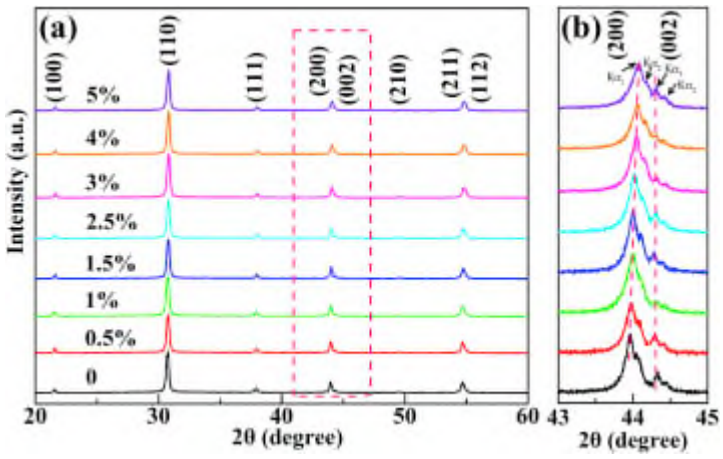

Fig. 2. (a) XRD patterns of PLZST ceramics with different La^{3+} contents. (b) Fine-scan XRD patterns of the PLZST ceramics in 2θ range of 43o-45°; Kα1 and Kα2 indicate the diffraction peaks from Cu Kα1 and Kα2 radiations (λKα1 = 1.5406 Å and λKα2 = 1.5444 Å), respectively.

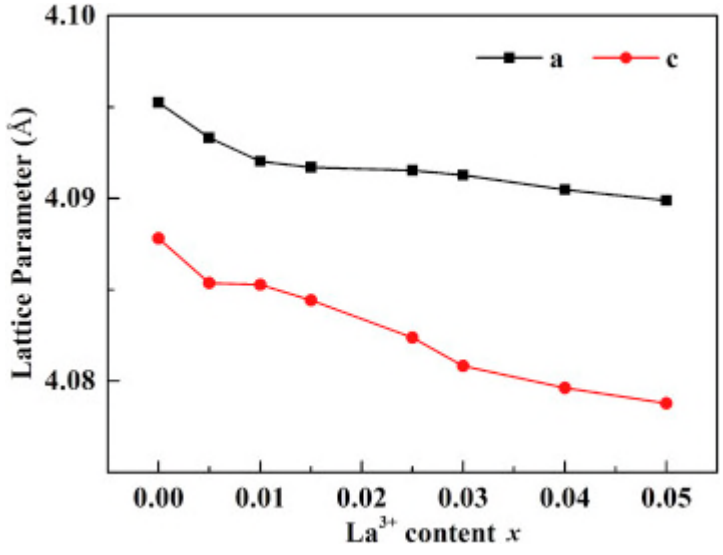

Fig. 3. Lattice parameters a and c of the PLZST ceramics with different La3+ contents.

Fig. 4(a)-4(h) show scanning electron micrographs of the fresh PLZST ceramics with various La3+ contents. The La3+ content distinctly affects the grain size. Upon increasing the La3+ content from x = 0 to 0.5%, the grain size clearly increases, which may be associated with the higher grain-growth rate caused by quicker diffusion of the smaller La3+ ion in place of the larger Pb2+ ion. As the La3+ content further increases, the ceramic grain size decreases obviously. Introducing additional La3+ leads to the formation of Pb2+ vacancies with a negative charge, which can be easily segregated at the grain boundary. These vacancies can attract the positively charged La3+ ion, thereby creating La-VPb" pairs near the grain boundary through Columbic interactions. These vacancy-aliovalent ion pairs impede the movement of the grain boundary and thus suppress the grain growth leading to reduced grain size [18,19]. In addition, when the La3+ content is less than 3 mol%, all ceramics have a dense microstructure, whereas pores start to appear upon further increasing the La3+ content to 4 mol%. Higher La3+ content leads to larger lattice distortion and thus more defects in the ceramics.

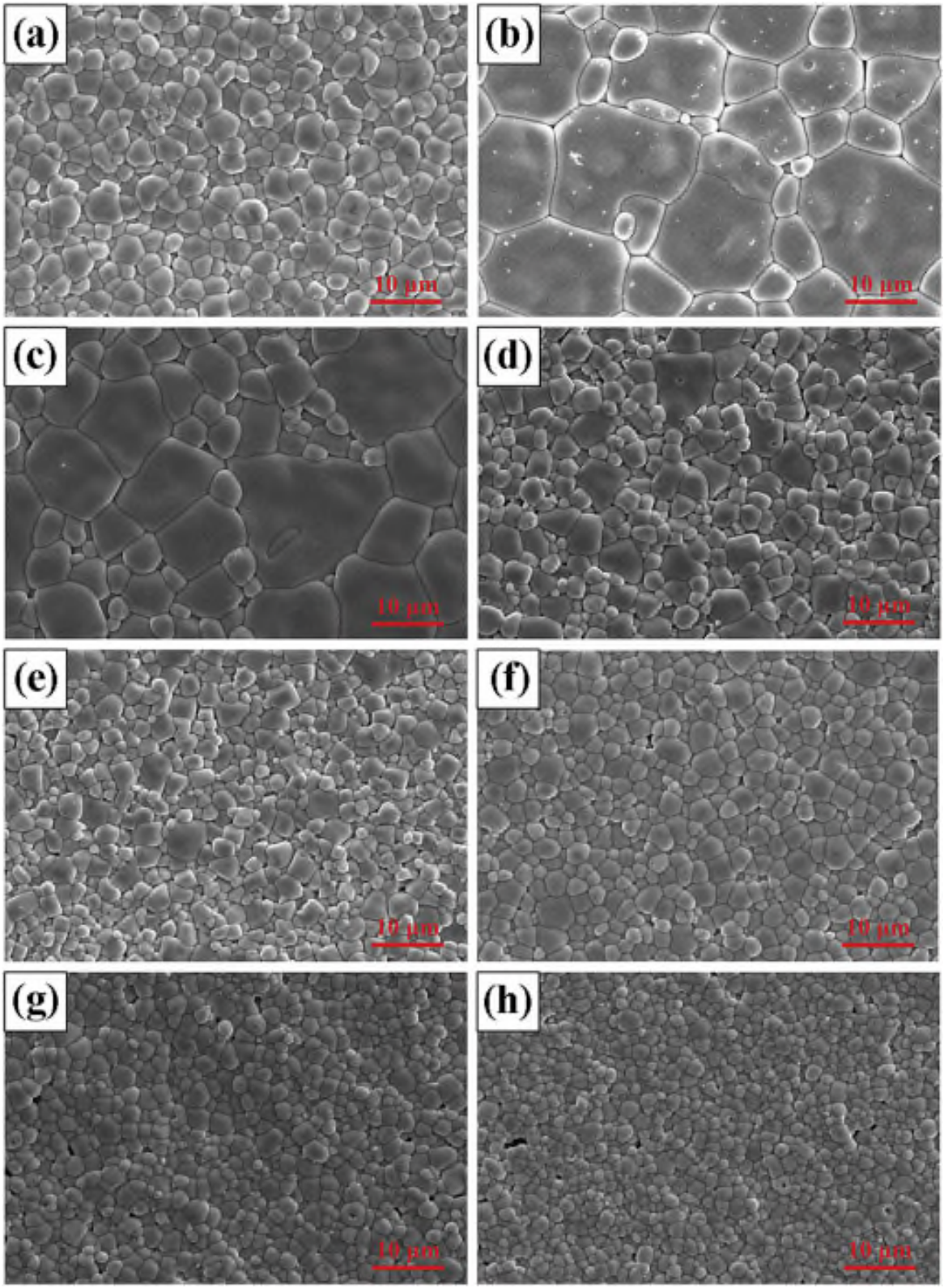

Fig. 4. SEM micrographs of (Pb1-1.5xLax)(Zr0.5Sn0.43Ti0.07)O3 ceramics with different La3+ contents: (a) x = 0, (b) x = 0.5%, (c) x = 1%, (d) x = 1.5%, (e) x = 2.5%, (f) x = 3%, (g) x = 4%, and (h) x = 5%.

Fig. 5 gives densities of the PLZST ceramics with different La3+ contents. As seen from the figure, when the La3+ content increases from x = 0 to x = 3%, both apparent and relative densities of the ceramics increase from 7.92 g/cm3 and 92% to 8.25 g/cm3 and 97%, respectively. This means that suitable La3+ content benefits the densification of ceramics during the sintering process. However, when the La3+ content is beyond 3 mol%, the apparent density and the relative density both decrease obviously, as a consequence of formation of pores in the ceramics as affirmed by the SEM observation.

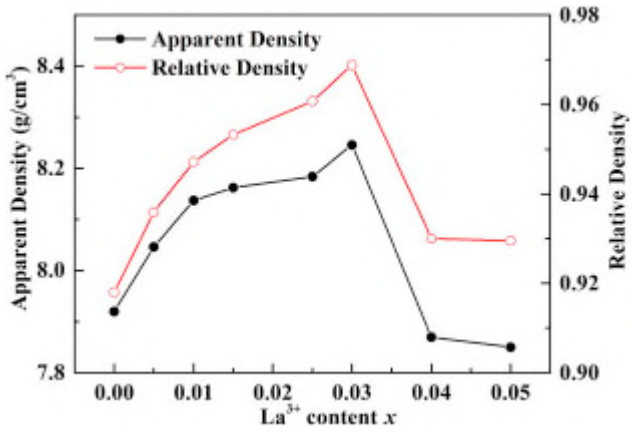

Fig. 5. The apparent density and relative density of the PLZST ceramics with different La3+ contents.

Elemental mappings of all ceramics were done using energy-dispersive spectrometry (FESEM/EDS). Fig. 6 displays representative EDS spectra along with a micrograph for the ceramic with x = 3%. All EDS spectra corresponding to various elements were recorded within the same area as in Fig. 6(a). As seen from Fig. 6(b)-6(g), all elements in the PLZST AFE ceramic are detected and evenly distributed without agglomeration. An integrated-area spectrum appears in Fig. 6(h) and is tabulated by atoms and the weight percentage of constituent elements. The atomic ratio given from the area EDS analysis is nearly the same as the stoichiometric formula of the ceramic, which is beneficial for obtaining superior energy-storage properties in this ceramic.

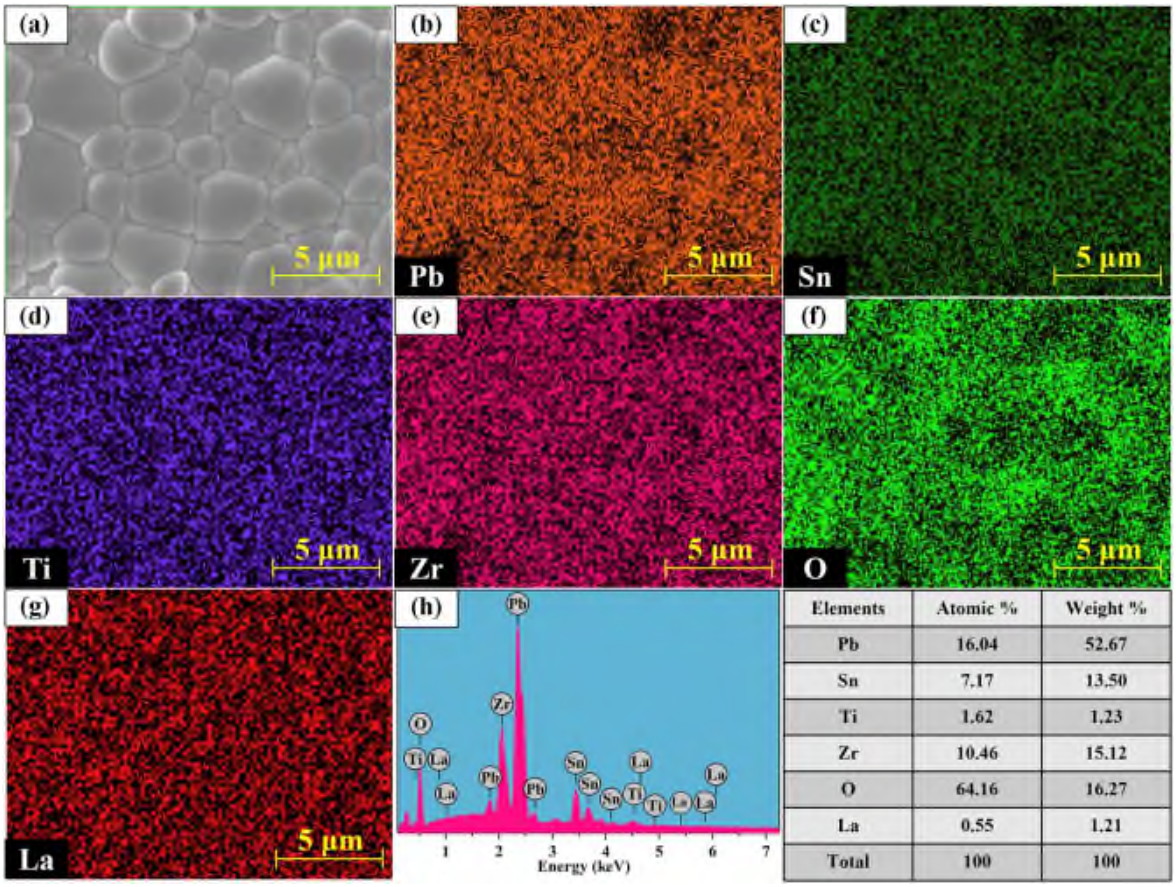

Elements	Atomic %	Weight %
Pb	16.04	52.67
Sn	7.17	13.50
Ti	1.62	1.23
Zr	10.46	15.12
O	64.16	16.27
La	0.55	1.21
Total	100	100

Fig. 6. FESEM-EDS elemental mapping of (Pb1-1.5xLax)(Zr0.5Sn0.43Ti0.07)O3 ceramics with x = 3%: (a) surface microstructure, and elementals mapping of (b) Pb, (c) Sn, (d) Ti, (e) Zr, (f) O, and (g) La. (h) EDS spectrum (left panel) and quantitative atomic and weight percent of various elements (right table).

The La3+ content not only affects the microstructure of PLZST AFE ceramics, but also may strongly influence the energy-storage properties. Therefore, it is desirable to find a suitable La3+ content for obtaining the best energy-storage characteristics. Fig. 7(a) and (b) show P-E hysteresis loops and current-electric field (I-E) curves, respectively, measured at 10 Hz and room temperature for all ceramics. Fig. 7(c) and (d) present EF, EA, ΔE, W, Wre, and η of the ceramics with various La3+ contents, where EF, EA, and ΔE are determined from the I-E curves, and W, Wre, and η are calculated from the P-E hysteresis loops. All ceramics exhibit double P-E hysteresis loops, confirming the AFE symmetry of these ceramics. Besides, as the La3+ content increases, Eb first increases and then decreases. Generally, the Pb-based ceramics

exhibit p-type conductivity due to the volatilization of PbO at high sintering temperature. In this study, La3+ ions with higher valence substituted for Pb2+ ions are considered as donor doping, which neutralizes the hole carriers and thus increases the electric resistivity and breakdown strength of the ceramic. The decrease of the Eb is attributed to the deterioration of the sintering behavior, as affirmed by the SEM observation above. In addition, when the La3+ content increases, the shapes of P-E hysteresis loops change from square to slim-slanted and become slimmer, indicating the reduction of the ΔE and thus the increase of the η. Moreover, as seen from Fig. 7(b) and (c), increasing the La3+ content clearly improves both EF and EA, which is on account of the enhancement of the AFE phase stability. Generally, the stability of the perovskite structure is evaluated by the tolerance factor t, which is expressed as [20]:(4)t=RA+RO2RB+RO, where RA, RB, and RO are respectively the ionic radii of A-site cation, B-site cation, and oxygen anion. The ferroelectric phase can be stabilized when the tolerance factor is more than 1, and the antiferroelectric phase can be stabilized when the tolerance factor is less than 1. The ionic radius of La3+ ions(1.36 Å) is smaller than that of Pb2+(1.49 Å), and thus substitution of La3+ for Pb2+ in the A-site will suppress the FE state and stabilize the AFE state. The increased EA, Eb and reduced ΔE contribute to the improved energy-storage properties, as seen in Fig. 7(d). When the La3+ content is 3 mol%, the ceramic exhibits optimum energy-storage characteristics, with a large Wre of 4.2 J/cm3 and a high η of 78%, which are respectively 2.9 and 1.56 times greater than those of (Pb1-1.5xLax)(Zr0.5Sn0.43Ti0.07)O3 AFE ceramics with x = 0 (Wre = 1.45 J/cm3, η = 50%). Upon further increasing the La3+ content to x = 4%, the energy-storage capacity of the ceramic drops because of the decreased Eb.

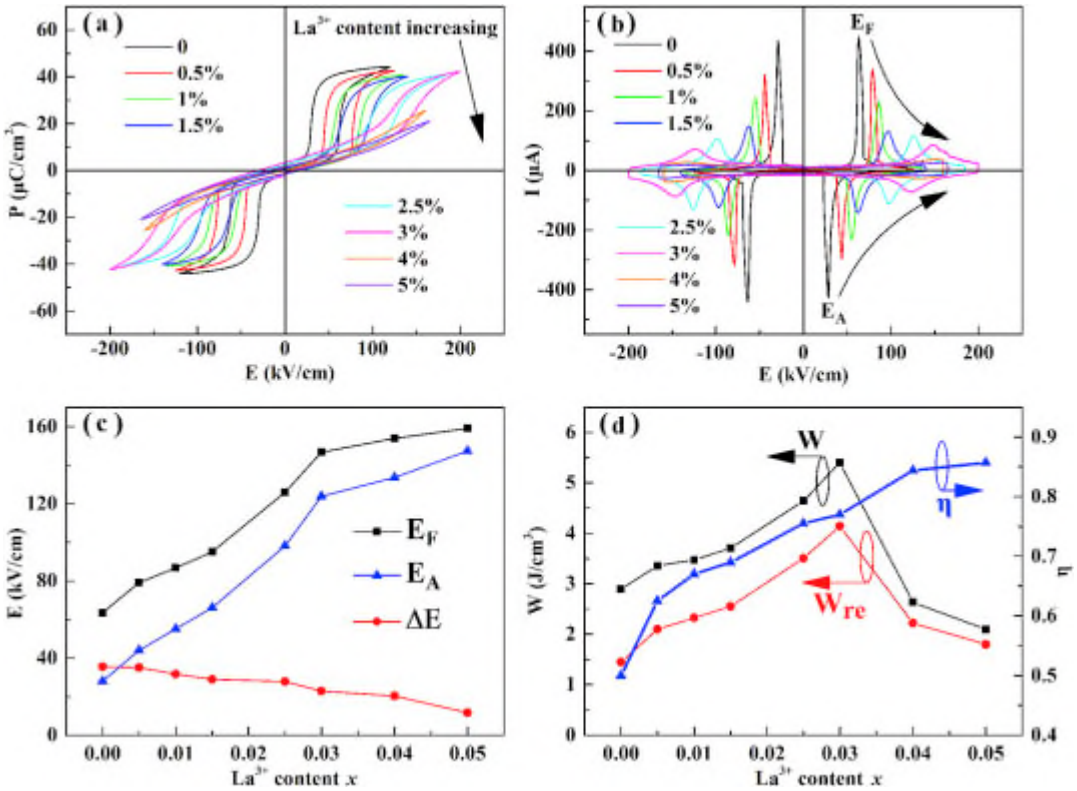

Fig. 7. (a) P-E hysteresis loops, (b) I-E curves, (c) EF, EA, ΔE, and (d) W, Wre, and η of PLZST ceramics with different La3+ contents.

Fig. 8 compares the room-temperature Wre and η of recently reported (Pb,La)(Zr,Sn,Ti)O3 AFE ceramics [[8], [9], [10], [11], [12],[21], [22], [23], [24], [25], [26], [27], [28]]. In previously reported work, it was hardly possible to acquire simultaneously large Wre and high η in a single material. For instance, (Pb0.858Ba0.1La0.02Y0.008)(Zr0.65Sn0.3Ti0.05)O3-(Pb0.97La0.02)(Zr0.9Sn0.05 Ti0.05)O3 AFE ceramics possess an excellent Wre of 6.40 J/cm3, whereas the η is only about 62.4% [21]. Conversely, Pb0.88La0.04Sr0.06[(Zr0.6Sn0.4)0.84Ti0.16]O3 AFE ceramics have a very high η of 93.3% but suffer from a low Wre of 1.52 J/cm3 [22]. In contrast, the Pb0.955La0.03(Zr0.5Sn0.43Ti0.07)O3 AFE ceramic in the present work has simultaneously a very large Wre and a fairly high η, which makes it overall superior to other lead-based AFE ceramics in terms of energy-storage properties.

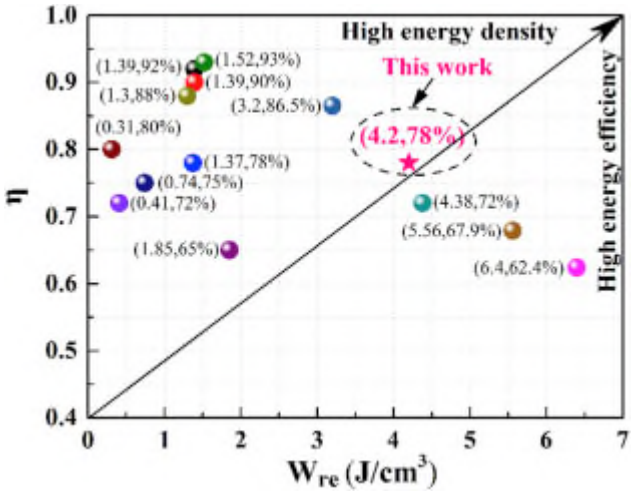

Fig. 8. Comparison of energy densities and efficiencies of recently reported (Pb,La)(Zr,Sn,Ti)O3 AFE ceramics.

Besides large Wre and high η, the temperature stability of the energy-storage characteristics is also of great importance for AFE materials, because dielectric capacitors always have to work over a wide range of temperatures in practical applications. For this reason, we further study in the following the influence of the temperature on energy-storage characteristics for 3 mol% La-doped $(Pb_{1-1.5x}La_x)(Zr_{0.5}\ Sn_{0.43}Ti_{0.07})O_3$ ceramics (see Fig. 9). As seen in Fig. 9(a), the ceramic exhibits typical double P-E hysteresis loops of AFE materials between 25 °C and 125 °C, and the hysteresis loops become slimmer with increasing measuring temperature. The Pmax, Pr, $\Delta P = Pmax - Pr$, EF, EA, and ΔE, which are determined from P-E hysteresis loops and I-E curves [Fig. 9(b)], are presented in Fig. 9(c) as functions of temperature. EF, EA, ΔE, and Pmax clearly decrease upon increasing the temperature. When the measurement temperature rises, the ceramic transforms from the AFE state gradually to paraelectric (PE) state, and thus the AFE phase stability reduces. This decreases the coupling strength between electric dipoles in the AFE state. In other words, the electric-dipole interaction energy Winter is reduced. In addition, increasing the temperature makes it easier for reorientation of electric dipoles, leading to the decrease of the strain energy Wstr. Hence, the EF, ΔE and Pmax, which are respectively proportional to Winter + Wstr, 2Wstr and the stability of AFE phase, reduce with the increase

of the measurement temperature. The reduction of the EA (proportional to Winter − Wstr) may be a result of faster decrease of the Winter than the Wstr [11]. The W, Wre, and η measured at 150 kV/cm and different temperature are given in Fig. 9(d). Clearly, in the temperature range of 25–125 °C, the Wre exceeds 2 J/cm3, the η is higher than 85%, and their variations are very slight, indicating good temperature stability. These results distinctly make (Pb1-1.5xLax)(Zr0.5Sn0.43Ti0.07)O3 AFE ceramics with 3 mol% content a potential candidate material for preparing power capacitors that can operate at a high temperature.

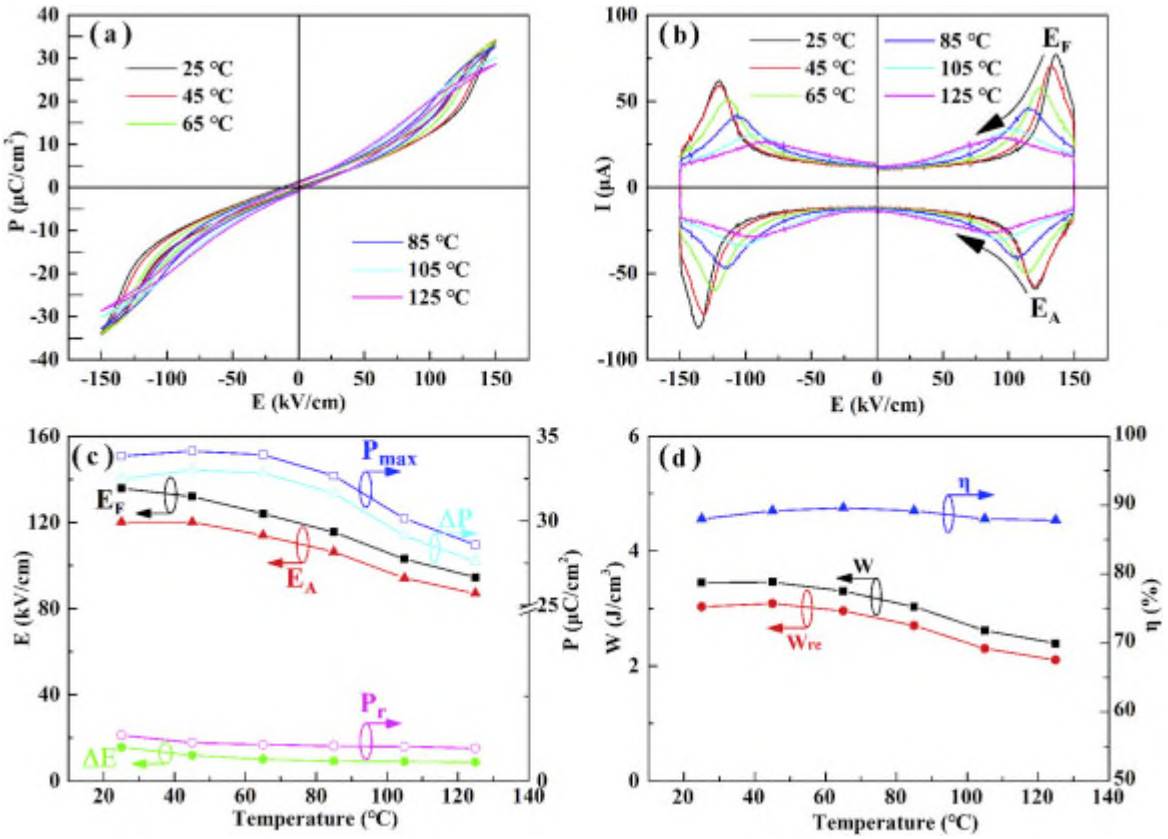

Fig. 9. (a) P-E hysteresis loops measured at 150 kV/cm, (b) I-E curves, (c) EF, EA, ΔE, Pmax, Pr and ΔP, and (d) W, Wre, and η of (Pb1-1.5xLax)(Zr0.5Sn0.43Ti0.07)O3 AFE ceramic with x = 3% in the temperature range of 25–125 °C.

4. Conclusions

In summary, we prepare (Pb1-1.5xLax)(Zr0.5Sn0.43Ti0.07)O3 AFE ceramics with different La3+ contents in the pure perovskite phase by the traditional ceramic fabrication method, and

then study how the La3+ content affects the crystal structure, microscopic morphology, and energy-storage properties of these ceramics. Upon increasing the La3+ content, the electric conductivity of the ceramic reduces, the AFE phase stability improves, and the AFE state gradually transforms to the relaxor AFE state with slimmer P-E hysteresis loops, which result in the increase of EA and Eb, and the decrease of ΔE. Thus, the Wre and η improve from 1.45 J/cm3 and 50% (x = 0) to 4.2 J/cm3 and 78% (x = 0.03). However, upon further increasing the La3+ content to 4 mol%, the Eb of the ceramic decreases because of the increase of pores, so the Wre reduces to 2.2 J/cm3. Besides, the Wre and η of the ceramic with 3 mol% La3+ show good temperature stability between 25 °C and 125 °C. These results indicate the potential of the Pb0.955La0.03(Zr0.5Sn0.43Ti0.07)O3 AFE material for fabricating advanced pulsed capacitors.

Acknowledgments

This work was supported by the NSFC (Nos. 51572073, 51602093, 11774082, 51872079), NSF of Hubei Province (Nos. 2016AAA031, 2018CFB700), Wuhan application foundation frontier Project (No. 2018010401011287), and State Key Laboratory of Advanced Technology for Materials Synthesis and Processing (Wuhan University of Technology; Grant No. 2018-KF-16).

References

[1] Z.H. Yao, Z. Song, H. Hao, Z.Y. Yu, M.H. Cao, S.J. Zhang, M.T. Lanagan, H.X. LiuHomogeneous/inhomogeneous-structured dielectrics and their energy-storage performances

Adv. Mater., 29 (2017), p. 1601727

[2] Q. Li, L. Chen, M.R. Gadinski, S. Zhang, G.Z. Zhang, H.U. Li, E. Iagodkine, A. Haque, L.Q. Chen, T.N. Jackson, Q. WangFlexible high-temperature dielectric materials from polymer nanocomposites
Nature, 523 (2015), p. 576

[3] Q. Li, K. Han, M.R. Gadinski, G.Z. Zhang, Q. WangHigh energy and power density capacitors from solution-processed ternary ferroelectric polymer nanocomposites
Adv. Mater., 26 (2014), pp. 6244-6249

[4] K. Han, Q. Li, C. Chanthad, M.R. Gadinski, G.Z. Zhang, Q. WangA hybrid material approach toward solution-processable dielectrics exhibiting enhanced breakdown strength and high energy density
Adv. Funct. Mater., 25 (2015), pp. 3505-3513

[5] B. Li, Q.Y. Liu, X.G. Tang, T.F. Zhang, Y.P. Jiang, W.H. Li, J. LuoAntiferroelectric to relaxor ferroelectric phase transition in PbO modified (Pb0.97La0.02)(Zr0.95Ti0.05)O3 ceramics with a large energy-density for dielectric energy storage RSC Adv., 7 (2017), p. 43327

[6] Z.Q. Hu, B.H. Ma, S.S. Liu, M. Narayanan, U. BalachandranRelaxor behavior and energy storage performance of ferroelectric PLZT thin films with different Zr/Ti ratios
Ceram. Int., 40 (2014), pp. 557-562

[7] Q.F. Zhang, J. Chen, Y.M. Lu, T.Q. Yang, X. Yao, Y.B. He(Pb,Sm)(Zr,Sn,Ti)O3 Multifunctional ceramics with large electric-field-induced strain and high-energy storage density
J. Am. Ceram. Soc., 99 (2016), pp. 3853-3856

[8] R. Xu, Z. Xu, Y.J. Feng, H.L. He, J.J. Tian, D. HuangTemperature dependence of energy storage in Pb0.90La0.04Ba0.04[(Zr0.7Sn0.3)0.88Ti0.12]O3 antiferroelectric ceramics
J. Am. Ceram. Soc., 99 (2016), p. 2984

[9] Q.F. Zhang, Y. Dan, J. Chen, Y.M. Lu, T.Q. Yang, X. Yao, Y.B. HeEffects of composition and temperature on energy storage properties of (Pb,La)(Zr,Sn,Ti)O3 antiferroelectric ceramics Ceram. Int., 43 (2017), pp. 11428-11432

[10] R. Xu, B.R. Li, J.J. Tian, Z. Xu, Y.J. Feng, X.Y. Wei, D. Huang, L.J. YangPb0.94La0.04[(Zr0.70Sn0.30)0.90Ti0.10]O3 antiferroelectric bulk ceramics for pulsed capacitors with high energy and power density Appl. Phys. Lett., 110 (2017), p. 142904

[11] Y. Dan, H.J. Xu, K.L. Zou, Q.F. Zhang, Y.M. Lu, G. Chang, H.T. Huang, Y.B. HeEnergy storage characteristics of (Pb,La)(Zr,Sn,Ti)O3 antiferroelectric ceramics with high Sn content Appl. Phys. Lett., 113 (2018), p. 063902

[12] Q.F. Zhang, H.F. Tong, J. Chen, Y.M. Lu, T.Q. Yang, X. Yao, Y.B. HeHigh recoverable energy density over a wide temperature range in Sr modified (Pb,La)(Zr,Sn,Ti)O3 antiferroelectric ceramics with an orthorhombic phase Appl. Phys. Lett., 109 (2016), p. 262901

[13] X. Chen, X. Dong, G. Wang, F. Cao, F. Hu, H. ZhangDielectric and ferroelectric properties of lanthanum-modified lead zirconate stannate titanate (42/40/18) ceramics
J. Am. Ceram. Soc., 101 (2018), pp. 3979-3988

[14] A.K. Yadav, A. Verma, S. Kumar, V. Srihari, A.K. Sinha, V.R. Reddy, S.W. Liu, S. Biring, S. SenInvestigation of La and Al substitution on the spontaneous polarization and lattice dynamics of the Pb(1-x)LaxTi(1-x)AlxO3 ceramics J. Appl. Phys., 123 (2018), p. 124102

[15] P. Liu, D. ZhangDielectric relaxation of (Pb(1-3x/2)Lax)(Zr0.5Sn0.3Ti0.2)O3 antiferroelectric ceramics induced by lanthanum doping Acta Phys. Sin., 1 (2011), p. 017701

[16] Y.J. Feng, Z. Xu, H.G. Li, X. YaoEffect of La modifier on the electric hysteresis of lead zirconate stannate titanate compounds Ceram. Int., 30 (2004), pp. 1393-1396

[17] F.P. Zhuo, Q. Li, Y.Y. Li, J.H. Gao, Q.F. Yan, Y.L. Zhang, X.C. Chu, W.W. CaoEffect of A-site La3+ modified on dielectric and energy storage properties in lead zironate stannate titanate ceramics

Mater. Res. Express, 1 (2014), p. 045501

[18] R.D. Levi, Y. TsurThe effect of oxygen vacancies in the early stages of BaTiO3 nanopowder sintering Adv. Mater., 17 (2005), pp. 1606-1608

[19] Z. Arif, H. Ali, M. Rizwan Ahmed, M. Adnan, N. Sahn, K. Myong HoDielectric and electromechanical properties of LiNbO3-modified (BiNa)TiO3-(BaCa)TiO3 lead-free piezoceramics

J. Phys. D Appl. Phys., 49 (2016), p. 175301

[20] Y.J. Yu, R.N. SinghEffect of composition and temperature on field-induced properties in the lead strontium zirconate titanate system J. Appl. Phys., 88 (2000), p. 7249

[21] L. Zhang, S.L. Jiang, B.Y. Fan, G.Z. ZhangEnhanced energy storage performance in (Pb0.858Ba0.1La0.02Y0.008)(Zr0.65Sn0.3Ti0.05)O3-(Pb0.97La0.02)(Zr0.9 Sn0.05Ti0.05)O3 anti-ferroelectric composite ceramics by spark plasma sintering

J. Alloy. Comp., 622 (2015), pp. 162-165

[22] R. Xu, Z. Xu, Y.J. Feng, J.J. Tian, D. HuangEnergy storage and release properties of Sr-doped (Pb,La)(Zr,Sn,Ti)O3 antiferroelectric ceramics Ceram. Int., 42 (2016), pp. 12875-12879

[23] C.H. Xu, Z. Liu, X.F. Chen, S.G. Yan, F. Cao, X.L. Dong, G.S. WangHigh charge-discharge performance of Pb0.98La0.02(Zr0.35Sn0.55Ti0.10)0.995O3 antiferroelectric ceramics

J. Appl. Phys., 120 (2016), p. 074107

[24] Z. Liu, X.F. Chen, W. Peng, C.H. Xu, X.L. Dong, F. Cao, G.S. WangTemperature-dependent stability of energy storage properties of Pb0.97La0.02(Zr0.58Sn0.335Ti0.085)O3 antiferroelectric ceramics for pulse power capacitors Appl. Phys. Lett., 106 (2015), p. 262901

[25] S.E. Young, J.Y. Zhang, W. Hong, X. TanMechanical self-confinement to enhance energy storage density of antiferroelectric capacitors J. Appl. Phys., 113 (2013), p. 054101

[26] H.L. Zhang, X.F. Chen, F. Cao, G.S. Wang, X.L. DongCharge-discharge properties of an antiferroelectric ceramics capacitor under different electric fields J. Am. Ceram. Soc., 93 (2010), p. 4015

[27] I.V. Ciuchi, L. Mitoseriu, C. GalassiAntiferroelectric to ferroelectric crossover and energy storage properties of (Pb1−xLax)(Zr0.90Ti0.10)1−x/4O3 ($0.02 \leq x \leq 0.04$) ceramics J. Am. Ceram. Soc., 99 (2016), p. 2382

[28] R. Xu, Z. Xu, Y.J. Feng, X.Y. Wei, J.J. Tian, D. HuangPolarization of antiferroelectric ceramics for pulse capacitors under transient electric field J. Appl. Phys., 119 (2016), p. 224103

2019-03-06

Superior energy-storage properties in (Pb,La)(Zr,Sn,Ti)O-3 antiferroelectric ceramics with appropriate La content

Dan, Yu

Elsevier

Dan Y, Zou K, Chen G, et al., (2019) Superior energy-storage properties in (Pb,La)(Zr,Sn,Ti)O-3 antiferroelectric ceramics with appropriate La content. Ceramics International, Volume 45, Issue 9, June 2019, pp.11375-11381

https://doi.org/10.1016/j.ceramint.2019.03.001